ISSN 0001-4338, Izvestiya, Atmospheric and Oceanic Physics, 2024, Vol. 60, No. 5, pp. 523–532. © Pleiades Publishing, Ltd., 2024.

Optical Characteristics of Atmospheric Aerosol Based on the Results of Measurements near St. Petersburg from 2016 to 2021

K. A. Shpak[a], *, E. Yu. Nebosko[a], and D. V. Ionov[a]

[a] *St. Petersburg State University, St. Petersburg, 199034 Russia*

**e-mail: k.shpak@spbu.ru*

Received March 19, 2024; revised June 4, 2024; accepted July 10, 2024

Abstract—This paper presents the results of measurements of the optical characteristics of aerosol particles using a solar photometer and nephelometer from 2016 to 2021 obtained at the atmospheric monitoring station in Peterhof (59.88° N, 29.83° E). The measurements are compared with the MERRA-2 reanalysis data. It is shown that interseasonal variability is observed in the region, characterized by low values of the Angstrom exponent in winter and high values in the warm season. The backscatter fraction has a similar—but less pronounced—seasonal cycle. The average value of the turbidity coefficient for the period is less than 0.10, which makes it possible to determine the observation station as a background one. Using the HYSPLIT model, the origin of air masses forming the atmospheric air state at the observation station is determined when the limiting values of the measured scattering coefficients (<10 and >70) and the Angstrom exponent (<1) are realized. Air masses coming from the northwest correspond to clean and humid air from the marine area and are manifested in the minimum values of the measured parameters. The maximum values of the scattering coefficient are associated with fine aerosol entering the atmosphere both from regional emissions sources (urban pollution from the territory of St. Petersburg) and as a result of transboundary transport from southwestern directions.

Keywords: scattering coefficient, Ångström exponent, atmospheric aerosol, nephelometer, sun photometer

DOI: 10.1134/S0001433824700518

1. INTRODUCTION

Aerosol particles are an important component of the atmospheric environment. Actively interacting with atmospheric components during the processes of coagulation and cloud formation and participating in chemical reactions and the absorption and scattering of solar radiation, aerosol affects weather and climate change on regional and global scales. The degree of involvement of atmospheric aerosol in certain processes depends on the size, shape, chemical composition, and number of particles. In this regard, continuous monitoring of changes in the characteristics of atmospheric aerosol in order to study their relationship with various climatic parameters is one of the most important tasks in atmospheric physics. Data from monitoring the optical characteristics of an aerosol are used both to determine its radiation properties and obtain an indirect assessment of the microphysical parameters of aerosol particles (Ångström, 1929; Eck et al., 1999; Delene and Ogren, 2002; Hansen et al., 2000; Mikhailov et al., 2006, Tami et al., 2006; Andreae and Rosenfeld, 2008; Jung et al., 2013; Smith and Bond, 2014).

Studying the variability of the content of the main gas components and aerosols is the main goal of creating an atmospheric monitoring station at the Geomodel resource center (RC) of St. Petersburg State University (e.g., Timofeyev et al., 2016; Foca et al., 2019). The observation tower is located in the city of Peterhof (59.88° N, 29.83° E), 29 km southwest of the center of St. Petersburg, which has a population of more than 5 million people. The environs of such large metropolitan areas are characterized by the accumulation of air pollution caused by intensive emissions from industrial enterprises and motor vehicles. Due to the peculiarities of its geographical location and depending on meteorological conditions (in particular, wind direction and the height of the boundary layer), Peterhof periodically finds itself in the zone of removal of polluted air masses from the territory of St. Petersburg, which leads to the alternation of urban and background conditions at the research station in question (Vlasenko et al., 2019, 2023; Ionov and Poberovsky, 2020).

Over the past decade, a fairly large volume of data from measurements of aerosol characteristics carried out in Peterhof has been analyzed, both in the surface layer (for example, the concentration of carbon-containing components and particulate matter) and in the atmospheric column (for example, aerosol optical thickness (AOT), Angstrom parameter) (Sviridenkov et al., 2014, 2017; Volkova et al., 2018, 2020; Vlasenko et al., 2019). Based on long-term observations, some

seasonal features of aerosol variability have been identified. According to studies based on measurement data with a thermal-optical analyzer, the ratio of elemental (EC) to organic carbon (OC) has a summer maximum, exceeding the minimum winter values by almost 3 times, and coinciding in time with the peak of the growing season. EC is characterized by minimum concentrations in summer, while OC has the lowest values recorded in the cold season (Vlasenko et al., 2019, 2023). An analysis of measured mass concentrations of PM1, PM2.5 and PM10 using the GRIMM aerosol spectrometer showed strong day-to-day variability with a predominance of particles smaller than 1 μm. The highest concentrations of PM10 (about 8 $\mu g/m^3$) are observed in winter (Volkova et al., 2020). Measurements made during the first 4 years of operation of the CIMEL CE 318 solar photometer of the international observation network AERONET, starting in 2013, generally agree well with the data of measurements of aerosol characteristics at nearby network stations (Dubovik et al., 2000a, Volkova et al., 2018). Since 2012, periodic and then regular measurements of scattering coefficients by surface aerosol particles began to be performed using the TSI Model 3563 Integrating Nephelometer. The first results of the analysis of data from nephelometric measurements of the scattering coefficient were presented in (Sviridenkov et al., 2014). Later, this analysis was supplemented with data on the average cosine of the scattering indicatrix of atmospheric aerosol (Sviridenkov et al., 2017). This paper presents the results of a comprehensive study of measurements of optical aerosol characteristics in Peterhof for the period from 2016 to 2021, both in the surface layer using a nephelometer and in the atmosphere using a CIMEL photometer.

2. RESEARCH METHODOLOGY. MEASURING EQUIPMENT

2.1. Nephelometer

The TSI 3563 Integrating Nephelometer is designed for ground-based studies of aerosol scattering properties by measuring total σ_{sp} and scattering into the rear hemisphere of light σ_{bsp} aerosol particles at three wavelengths (450, 550, and 700 nm) (Anderson and Ogren, 1998). Aerosol samples are taken at the observation station of St. Petersburg State University from a height of 50 m above sea level.

Measurements of the aerosol scattering coefficient at several wavelengths make it possible to proceed to finite differences and calculate the scattering Angstrom parameter (indicator) α_s:

$$\alpha_{S\lambda_1}(\lambda_2) = -\frac{\log\dfrac{\sigma_{sp}(\lambda_2)}{\sigma_{sp}(\lambda_1)}}{\log\dfrac{\lambda_2}{\lambda_1}}. \quad (1)$$

In this work, wavelengths of 450 and 700 nm are used as λ_1 and λ_2.

The value of the Angstrom scattering index significantly depends on the particle size, which allows it to be used as an estimate of the effective particle size. A value of 4 indicates nanometer-sized particles, while values near 0 indicate the presence of large particles (Anderson and Ogren, 1998; Weber et al., 2022).

Using a parametric approach to the ratio of the scattering coefficient in the rear hemisphere to the total scattering coefficient b_λ ($b_\lambda = \dfrac{\sigma_{bsp}(\lambda)}{\sigma_{sp}(\lambda)}$) (hereinafter referred to as the backscattering fraction), the asymmetry factor g_λ can be calculated (Andrews et al., 2006; Sviridenkov et al., 2017; Zhao et al., 2018):

$$g_\lambda = 1 - \left(1.18/b_\lambda - 1.2\right)^{-0.49}. \quad (2)$$

Taking values from −1 to 1, the asymmetry factor characterizes the elongation of the scattering indicatrix. Limiting cases correspond to an indicatrix, which has the form of a forward or backward directed delta function. At zero value, the indicatrix is spherical and, therefore, radiation is scattered uniformly in all directions (Horvath et al., 2015).

2.2. Solar Photometer

The CIMELCE 318 solar photometer, part of the global aerosol monitoring network, records the intensities of direct and diffuse solar radiation in the solar almucantar and in the main solar plane at nine spectral channels (340, 380, 440, 500, 675, 870, 940, 1020, and 1640 nm). The device is installed on a tower at an altitude of 58 m above sea level. Photometer measurement data is interpreted by standard algorithms at the AERONET Processing Center (GSFC) (Eck et al., 1999; Dubovik et al., 2000a, 2000b; Schuster et al., 2006; Giles et al., 2019) based on an analysis of the spectral attenuation of radiation by the atmosphere, taking into account its scattering and absorption by aerosol particles.

AOT τ_λ is estimated by subtracting from the total optical depth the contributions of molecular (Rayleigh) scattering, as well as the molecular absorption of ozone and some other trace gas components (NO2, CO2, and CH4) (Holben et al., 1999, 2001). The spectral dependence of AOT is determined by the empirical Ångström expression $\tau_\lambda = \beta\lambda^{-\alpha}$ (Ångström, 1964; Stefan et al., 2011; Imashev, 2012), where β is the Angstrom turbidity coefficient equal to AOT at a wavelength of 1 μm and α is the Angstrom parameter, actually calculated as the angle of inclination between the logarithms of the specified parameters τ_λ and λ (Eck et al., 1999; Schuster et al., 2006). The calculation of the latter is included in the standard interpretation of AERONET data. Thus, for two wavelengths,

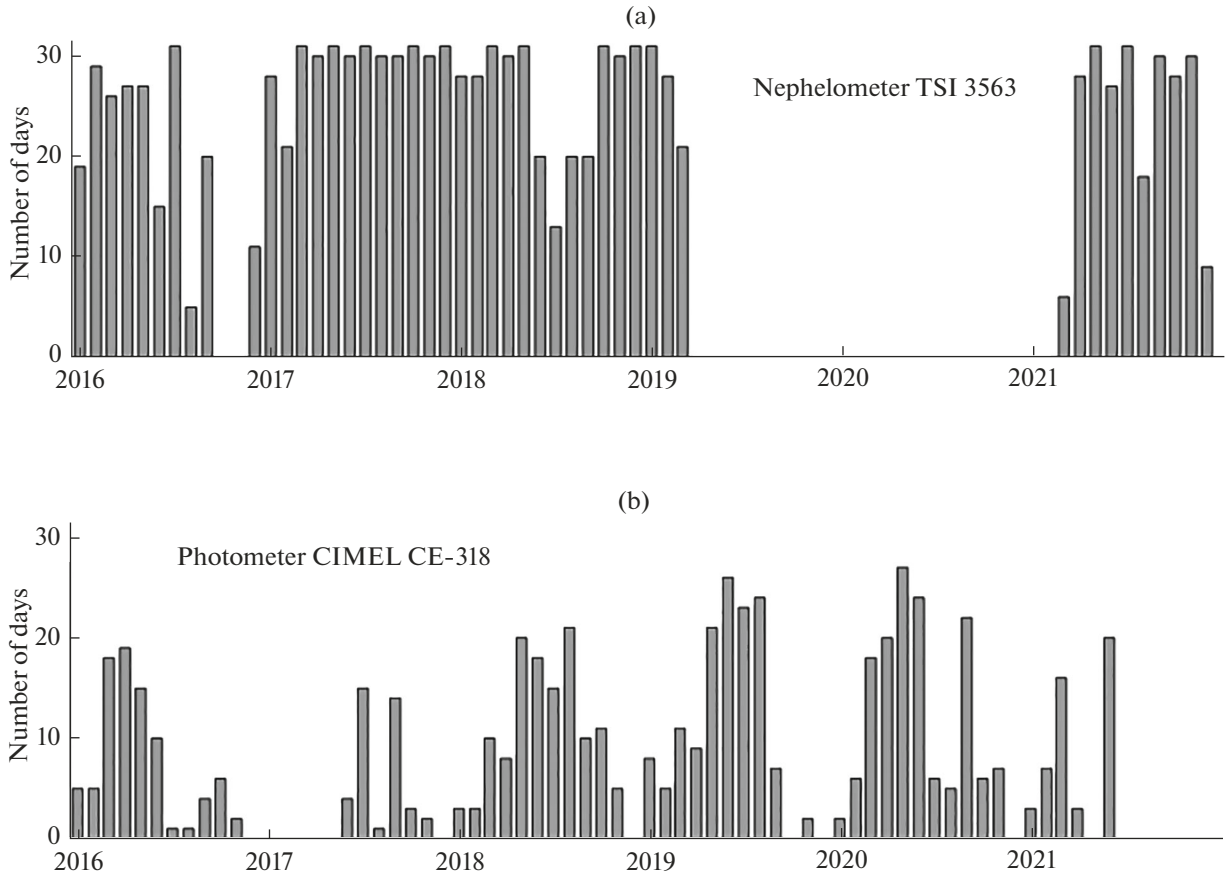

Fig. 1. Distribution by month of the number of days with measurements at the monitoring station in Peterhof (St. Petersburg) for 2016–2021: statistics are presented for the (a) nephelometer and (b) solar photometer.

the Ångström parameter and the turbidity coefficient are found as follows:

$$\alpha_{\lambda_1}(\lambda_2) = -\frac{\ln(\tau_{\lambda_2}/\tau_{\lambda_1})}{\ln(\lambda_2/\lambda_1)}, \quad (3)$$

$$\beta_{\lambda_1}(\lambda_2) = \tau_{\lambda_2}\lambda_2^{\alpha_{\lambda_1}(\lambda_2)}. \quad (4)$$

The Angstrom attenuation index varies depending on particle size, shape, and chemical composition. Its variability allows us to estimate the average size of aerosol particles in the atmosphere. As with the Angstrom scattering exponent, the values $\alpha \le 1$ indicate the predominance of the large mode (radius >0.5 μm) in the particle size distribution; when $\alpha \ge 2$, fine aerosol dominates (radius ≤ 0.5 μm) (Eck et al., 1999; Schuster et al., 2006). The turbidity coefficient is related to the number of aerosol particles and characterizes the degree of atmospheric pollution. Usually, the values of $\beta \le 0.1$ correspond to conditions of a clean atmosphere, and values of $\beta \ge 0.4$ correspond to heavily polluted conditions (Ångström, 1964).

Photometric measurements in solar almucantars provide information about the angular distribution of scattered radiation, the so-called phase scattering function $P(\theta)$, where θ is the scattering angle. Knowing $P(\theta)$ allows one to calculate the asymmetry factor g_λ, which is the average cosine of the scattering angle, weighted by the intensity of the scattering light as a function of angle. It takes the value 1 for forward scattering, 0 for isotropic scattering, and –1 for perfect backscattering. The degree of elongation of the scattering indicatrix depends on the particle size and refractive index.

3. MEASUREMENT RESULTS

3.1. Measurement Statistics

Figure 1 shows the distribution by month of the number of days with measurements by a nephelometer and a solar photometer at the Peterhof station.

Solar photometer measurements undergo a measurement rejection system standardized within the AERONET network, taking into account the influence of various factors, primarily the presence of cirrus clouds, smog, solar eclipses, atmospheric temperature anomalies, and weak spectral dependence of AOT. The statistics presented in Fig. 1 correspond to the selected AERONET data, the so-called level 2.0

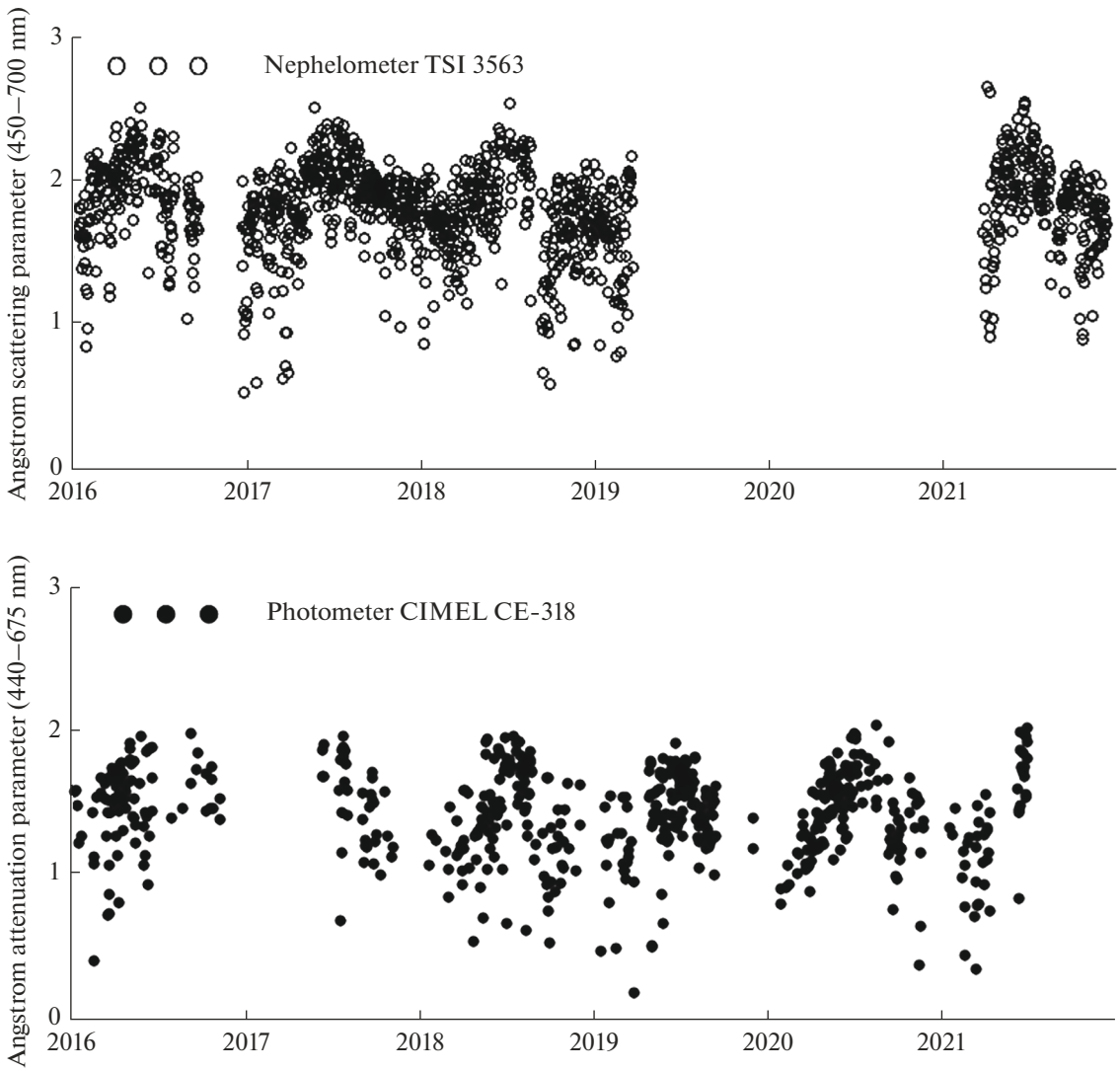

Fig. 2. Median daily values of the scattering Angstrom parameter at wavelengths of 450–700 nm according to nephelometer measurements (open circles) and the attenuation Angstrom parameter at wavelengths of 440–675 nm according to solar photometer measurements (black circles).

version 3.0 (Giles et al., 2019). The distribution of data over time is uneven: the number of individual measurements ranges from several to 50–60 per day; on average, about 30 measurements per day are recorded. The largest number of measurements occurs in the spring–summer period, which corresponds to favorable weather observation conditions. The absence of data in 2017 and 2021 is associated with sending equipment for calibration to the Mauna Loa Observatory (United States).

Unlike a photometer, continuous measurement data with a nephelometer is recorded every 5 min, regardless of weather conditions, with subsequent averaging of the data over an hour. Thanks to this, the nephelometer measurement data series is more homogeneous, and the number of days with measurements on average corresponds to the number of days in a month. The lack of nephelometer measurements in 2019–2021 is due to a technical malfunction of the device.

An analysis of the measurement results of two instruments, a photometer and a nephelometer, makes it possible to compensate for the lack of data from one instrument with the data of the other (if not quantitatively, then qualitatively) to identify the characteristic features of optical aerosol parameters.

3.2. Seasonal Features of the Optical Parameters of Aerosols

During the work, the median daily values of the Angstrom parameter were calculated based on nephelometer and photometer measurements for the period 2016–2021 (Fig. 2). Close wavelength intervals were

selected for both devices: 450–700 nm for a nephelometer and 440–675 nm for a photometer.

The average value and standard deviation (RMS) according to the nephelometer data for the entire period was 1.82 ± 0.32 and, according to the photometer, 1.42 ± 0.32. The correlation coefficient between the data of the two instruments was calculated based on 263 pairs and amounted to 0.66. In this case, the minimum correlation is observed in winter and the maximum is in spring. The value of the Angstrom index experiences strong day-to-day variability, apparently due to both proximity to potential sources of pollution and the geographical features of the observation region with frequent changes in air masses. At the same time, both series of measurement data for the Angstrom index demonstrate a pronounced seasonal variation: in the cold season, minimum values are observed (up to 0.54 for the nephelometer and 0.19 for the photometer) and, in summer, maximum values (up to 2.66 and 2.04, respectively).

Seasonal variability of the Angstrom parameter is clearly visible in the monthly average data, which are presented in Fig. 3.

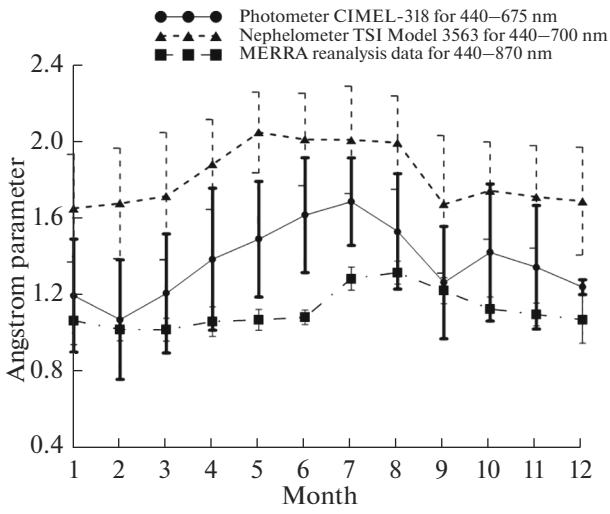

Fig. 3. Average monthly values of the Angstrom parameter according to measurements of the nephelometer (scattering, 450–700 nm), CIMEL photometer (attenuation, 440–675 nm), and according to MERRA-2 reanalysis data (attenuation, 440–870 nm).

In addition to the averaged nephelometer and photometer measurement data, the figure also shows MERRA-2 (Modern-Era Retrospective analysis for Research and Applications) reanalysis data on the Angstrom attenuation index in the atmosphere, calculated based on the assimilation of global experimental data for wavelengths of 440–870 nm (Rienecker et al., 2011). The average monthly values of the Angstrom index are obtained from a series of global MERRA-2 data (2016–2021) with a spatial resolution of 0.5° latitude × 0.625° longitude, generated for the coordinates of the observation station using the Giovanni Internet resource (https://giovanni.gsfc.nasa.gov). The average annual value of the Angstrom indicator according to MERRA-2 data for the entire period was 1.12 ± 0.12.

Interseasonal variability, characterized by low values of the Angstrom index in the cold season and high values in the warm season, is observed both in the results of ground-based measurements and in the reanalysis data. The MERRA-2 data, compared to the photometer and nephelometer measurement data, is characterized by the smallest amplitude of both average monthly values and seasonal variability of the Angstrom index. The nephelometer measurement data systematically exceeds the reanalysis data. This is probably explained by the fact that the MERRA-2 reanalysis data, which is based on the results of global satellite measurements, has a coarser spatial and temporal resolution. In nephelometric measurements of aerosol scattering coefficients, surface air samples are analyzed, and the corresponding observations are local and continuous. The monthly averages calculated from MERRA-2 data and obtained from measurements with the CIMEL photometer have close annual averages. Both data sources provide information on the content of aerosol particles throughout the atmosphere, taking into account the full spectral attenuation of solar radiation. The greatest discrepancies are observed from May to July. It is also worth noting the differences in the wavelength intervals used to calculate the analyzed Angstrom index; for ground-based instruments it is narrower (maximum 440–700 nm).

Qualitatively, the annual variation of the Ångström exponent according to ground-based measurements is in good agreement. The best agreement within the confidence intervals is observed from June to November. Apparently, the determining factor in the nature of its seasonal variability is the contribution of surface aerosols. Their concentration, in turn, is determined by terrestrial anthropogenic and natural sources, features of the underlying surface, and meteorological factors. Taking into account that in the nephelometric measurements of the Ångström parameter only the scattering component is taken into account and in the photometer measurements the complete attenuation of solar radiation by the atmosphere is considered, it can be assumed that the absorbing component of the Ångström parameter does not have a noticeable seasonal variation.

According to the interpretation of the inverse dependence of the Ångström parameter on particle size (Schuster et al., 2006), a shift in aerosol size towards the fine mode is observed in the summer months. First and foremost, this is due to an increase in insolation. The seasonal vegetation of plants and the warming of the earth's surface lead to the generation of the organic component of the aerosol. Against the background of rising temperatures in the plume of emissions from anthropogenic sources, photochemi-

Table 1. Average seasonal values of optical parameters (Angstrom parameter $\alpha_{440}(675)$, Angstrom scattering parameter $\alpha_{S450}(700)$, turbidity parameter $\beta_{440}(675)$, backscatter fraction b_{450}, AOT τ_{500}, and asymmetry factors g_{450} and g_{450}) according to measurements from a photometer (Cimel 318), and a nephelometer (TSI 3563) in Peterhof

Season	Parameters						
	$\alpha_{440}(675)$ Cimel 318	$\alpha_{S450}(700)$ TSI 3563	$\beta_{440}(675)$ Cimel 318	b_{450}, $\times 10^{-1}$ TSI 3563	τ_{500} Cimel 318	g_{450} TSI 3563	g_{440} Cimel 318
Winter	1.13 ± 0.29	1.67 ± 0.28	0.04 ± 0.03	1.08 ± 0.14	0.09 ± 0.05	0.67 ± 0.02	–
Spring	1.37 ± 0.31	1.87 ± 0.32	0.04 ± 0.02	1.21 ± 0.13	0.09 ± 0.06	0.65 ± 0.02	0.67 ± 0.03
Summer	1.59 ± 0.25	2.01 ± 0.25	0.04 ± 0.02	1.18 ± 0.16	0.12 ± 0.07	0.66 ± 0.03	0.68 ± 0.02
Autumn	1.32 ± 0.29	1.75 ± 0.31	0.04 ± 0.04	1.15 ± 0.16	0.11 ± 0.12	0.66 ± 0.03	0.70 ± 0.02

cal processes and chemical transformations from the gas phase in situ are activated with the formation of a secondary aerosol. The reasons for the increase in the number of large particles in winter may be the emission of particles with the onset of the heating season, which, under conditions of high relative humidity, lead to the coagulation of aerosol particles and their hygroscopic growth (Vlasenko et al., 2019).

Table 1 shows the average values and standard deviations of the main optical characteristics for the observation region in different seasons according to data from two instruments.

Related to the angular distribution of scattered radiation, indicator b_{450} and the asymmetry factor calculated on its basis g_{450} have a weakly expressed seasonal pattern. In winter, the values of b_{450} are minimum and those of g_{450} are maximum. The values of parameter g_{440} obtained from solar photometer measurements have no statistically supported data for the winter period. For the remaining seasons, the photometer measurement results provide numerical agreement with the nephelometer measurement data. Both parameters are functions of the angle, and the characteristic behavior over the period under consideration indicates the influence of larger aerosol in the cold season and the predominance of fine particles in summer (Horvath et al., 2015; Sviridenkov et al., 2017). Finnish researchers (Virkkula et al., 2011) obtained similar seasonal features of the backscattering fraction and the Ångström parameter. The minimum values observed in winter indicated an increase in anthropogenic emissions from seasonal heating with wood and coal, both in Finland and in Eastern Europe during the cold season.

Turbidity coefficient value $\beta_{440}(675)$ serves as a quantitative criterion for the cleanliness of the atmosphere in the observation region; a constant value less than 0.10 throughout the year characterizes the observation station as a background one, remote from intensive sources of emissions. Over the entire observation period, no more than 5% of single measurements were recorded with turbidity coefficient values from 0.10 to 0.40. The greatest variability of values $\beta_{440}(675)$, like AOT at 500 nm, is observed in autumn; the standard deviation during the season is comparable to the average value. This feature is associated, first and foremost, with changes in meteorological conditions in the fall: increasing cyclonic activity leads to the predominance of cloudy weather with drizzling rain and gusts of wind. At the same time, the height of the boundary layer becomes lower, which contributes to the accumulation of anthropogenic pollution in the surface layer (Volkova et al., 2020).

3.3. Trajectory Analysis

In order to assess the possible transformation processes in the chemical and structural composition of the aerosol on its way from the supposed sources to the observation station, it is necessary to analyze the history of the formation of the air mass under study. In this analysis, limiting cases with minimum and maximum values of optical characteristics were considered.

Using the HYSPLIT (HYbrid Single-Particle Lagrangian Integrated Trajectories (Draxler et al., 1998)) trajectory model, the reverse trajectories of air masses at the middle height of the boundary layer were calculated with a time step of 1 to 12 h back. The resulting ensembles of curves (total number of trajectories 1171) were combined into clusters of preferential directions, which are presented in Fig. 4.

Figure 4 presents the average air trajectories with their percentage distribution by direction for those observation days when the scattering Angstrom parameter according to nephelometer measurements was less than 1 (4% of all measurements). The measurement data and the estimated time of arrival of air masses at the observation point correspond to 12:00 UT. In 80% of measurement days, low values ($\alpha_{S450}(700) < 1$) are accompanied by minimum values of the measured total and backscattering coefficients. The average value of $\sigma_{sp}(550)$ was 6.16 ± 2.22 for this data sample, and the average value of $\sigma_{bsp}(550)$ was 0.86 ± 0.32. In the trajectory curves, two main directions are distinguished, southwestern and northwestern, correspond-

Fig. 4. Clusters of reverse trajectories of air mass movement according to calculation data of the HYSPLIT model for days with minimum values $\alpha_{S450}(700)$ less than 1.

ing to the waters of the Baltic Sea (together they describe 91% of all trajectories). According to the location of the initial points of the return trajectories presented in the figure, there are no air masses in the eastern and southern sectors of the directions in the ensemble. The sea surface, which is a natural source of easily soluble and hygroscopic aerosol particles with a radius of up to tens of micrometers, is simultaneously removed from the sources of industrial emissions of secondary fine aerosol. Therefore, air masses coming from remote sea areas are characterized by a predominance of coarse aerosol, confirmed by low values of the scattering Angstrom parameter.

Similar studies were previously carried out based on measurement data from the Finnish SMEAR II and Pallas observation stations (Virkkula et al., 2011; Aaltonen et al., 2006). A statistical analysis of the back trajectories for these stations showed that the clearest atmospheric conditions were associated with air masses originating in the Arctic Ocean and North Atlantic. These directions corresponded to the lowest average values of the scattering Angstrom parameter and the total and backscattering coefficients.

In turn, the measurement conditions with the highest values of the Angstrom parameter, as well as scattering and absorption coefficients, according to the studies conducted, were associated with sources of the corresponding aerosol in Central or Eastern Europe (Virkkula et al., 2011), as well as in the Russian industrial zone of the Kola Peninsula (Aaltonen et al., 2006).

An analysis of measurement data with a scattering Angstrom parameter value greater than 2 does not allow us to determine the location of potential sources of detected particles, since the calculated return trajectories indicate the arrival of the corresponding air masses from all possible directions.

Figure 5 shows clusters of reverse trajectories of air mass movement in the limiting case of high values of the total dispersion coefficient (more than 70), constituting 8% of all measurements. This threshold value was chosen empirically, based on mapping ensembles of back trajectories using various criteria for the value of σ_{sp}, in order to localize the supposed sources of characteristic air masses. Average values of $\sigma_{sp}(550)$ and $\sigma_{bsp}(550)$ are equal to 96.61 ± 35.53 and 10.66 ± 5.04, respectively.

The curves shown in the figure describe three predominant directions: south-southwest, southeast, and northeast, while 59% of all trajectories lie in the southern sector and indicate the continental origin of the corresponding air masses. The length of the curve of the northeastern cluster (35% of trajectories) is about 120 km, which indicates a low average wind

Fig. 5. Clusters of reverse trajectories of air mass movement according to calculation data of the HYSPLIT model for days with high values $\sigma_{sp}(550)$ (more than 70) according to nephelometer measurements.

speed and short-range transport of air masses. The reverse trajectories of this sector of directions cross the territory of the urban agglomeration of St. Petersburg, which may indicate the likelihood of a significant contribution of anthropogenic sources to air pollution at the observation station. High values of $\sigma_{sp}(550)$ corresponds to the average level of the Angstrom parameter, 1.71 ± 0.29. The latter indicates the presence of sources of aerosol particles with a polydisperse size distribution with a shift towards the dominance of the fine mode. These can be both regional sources (the removal of anthropogenic pollution from the territory of St. Petersburg or its southern suburbs) and the long-distance transport of solid particles from Eastern Europe.

CONCLUSIONS

Data from ground-based measurements of the main optical parameters of the atmosphere using the CIMEL CE 318 solar photometer and the TSI Model 3563 nephelometer near St. Petersburg from 2016 to 2021 were analyzed. It is shown that the annual variation of the Angstrom parameter has a pronounced character, with a maximum in summer and a minimum in the cold season. At the same time, the results of measurements with a nephelometer systematically exceed the data of measurements with a photometer: the average values of the Ångström parameter are 1.82 ± 0.32 and 1.42 ± 0.32, respectively. A comparison of observational results with MERRA-2 reanalysis data demonstrates close quantitative agreement with solar photometer measurements, in contrast to nephelometric measurement data. The discrepancies are apparently associated with significant differences in the spatio-temporal resolution of the data being compared, the maximum in the nephelometer measurements, and the minimum (rough) in the MERRA-2 data. Share backscattering has a summer maximum of 0.121 ± 0.013 and a winter minimum of 0.108 ± 0.014. Asymmetry factor g_{450}, calculated on the basis of measurement data with a nephelometer, has an average annual value of 0.66 ± 0.02, comparable to the results of measurements with a solar photometer. The seasonal variability of the parameters indicates that in the warm season there is a shift of the characteristic aerosol size toward the fine-dispersed mode, which may be associated with the activation of photochemical processes and the generation of secondary aerosol.

Based on calculations of the HYSPLIT model, clusters of reverse trajectories of air mass movement were studied for cases with values of measured scattering coefficients <10 and >70 and the Ångström parameter <1. The minimum parameter values are

typical for air masses coming from the northwestern direction, which corresponds to clean and humid air from the sea. The maximum values of the dispersion coefficient are associated with fine aerosol entering the atmosphere both from regional emission sources (urban pollution from the territory of St. Petersburg) and as a result of transboundary transport from southwestern directions.

FUNDING

This work was carried out with the support of St. Petersburg State University, project code 103752493. We used equipment from the Geomodel Research Center at the St. Petersburg State University Research Park for measurements.

CONFLICT OF INTEREST

The authors of this work declare that they have no conflicts of interest.

REFERENCES

Aaltonen, V., Lihavainen, H., Kerminen, V.-M., Komppula, M., Hatakka, J., Eneroth, K., Kulmala, M., and Viisanen, Y., Measurements of optical properties of atmospheric aerosols in Northern Finland, *Atmos. Chem. Phys.*, 2006, vol. 6, pp. 1155–1164.

Anderson, T.L. and Ogren, J.A., Determining aerosol radiative properties using the TSI 3563 integrating nephelometer, *Aerosol Sci. Technol.*, 1998, vol. 29, no. 1, pp. 57–69.

Andreae, M.O. and Rosenfeld, D., Aerosol–cloud–precipitation interactions. Part 1. The nature and sources of cloud-active aerosols, *Earth Sci. Rev.*, 2008, vol. 89, pp. 13–41.

Andrews, E., Sheridan, P.J., Fiebig, M., McComiskey, A., Ogren, J.A., Arnott, P., Covert, D., Elleman, R., Gasparini, R., Collins, D., Jonsson, H., Schmid, B., and Wang, J., Comparison of methods for deriving aerosol asymmetry parameter, *J. Geophys. Res.*, 2006, vol. 111, no. D5.

Ångström, A., On the atmospheric transmission of sun radiation and on dust in the air, *Geog. Ann.*, 1929, vol. 11, p. 156.

Ångström, A., The parameters of atmospheric turbidity, *Tellus*, 1964, vol. 16, no. 1, pp. 64–75.

Bond, T.C. and Bergstrom, R.W., Light absorption by carbonaceous particles: An investigative review, *Aerosol Sci. Technol.*, 2006, vol. 40, no. 1, pp. 27–67.

Delene, D.J. and Ogren, J.A., Variability of aerosol optical properties at four North American surface monitoring sites, *J. Atmos. Sci.*, 2002, vol. 59, pp. 1135–1150.

Draxler, R.R. and Hess, G.D., An overview of the hysplit-4 modelling system for trajectories, dispersion and deposition, *Aust. Meteorol. Mag.*, 1998, vol. 47, no. 4, pp. 295–308.

Dubovik, O. and King, M.D., A flexible inversion algorithm for retrieval of aerosol optical properties from Sun and sky radiance measurements, *J. Geophys. Res.*, 2000, vol. 105, pp. 20673–20696.

Dubovik, O., Smirnov, A., Holben, B., King, M., Kaufman, Y., Eck, T., and Slutsker, I., Accuracy assessments of aerosol optical properties retrieved from Aerosol Robotic Network (AERONET) sun and sky radiance measurements, *J. Geophys. Res.*, 2000, vol. 105, no. 8, pp. 9791–9806.

Eck, T.F., Holben, B.N., Reid, J.S., Dubovik, O., Smirnov, A., O'Neill, N.T., Slutsker, I., and Kinne, S., Wavelength dependence of the optical depth of biomass burning, urban and desert dust aerosols, *J. Geophys. Res.*, 1999, vol. 104, pp. 31333–31350.

Foka, S.Ch., Makarova, M.V., Poberovskii, A.V., and Timofeev, Yu.M., Temporal variations of CO_2, CH_4, and CO concentrations in the suburb of Saint-Petersburg (Peterhof), *Opt. Atmos. Okeana*, 2019, vol. 32, no. 10, pp. 860–866.

Giles, D.M., Sinyuk, A., Sorokin, M.G., Schafer, J.S., Smirnov, A., Slutsker, I., Eck, T.F., Holben, B.N., Lewis, J.R., Campbell, J.R., Welton, E.J., Korkin, S.V., and Lyapusti, A.I., Advancements in the Aerosol Robotic Network (AERONET) Version 3 database: Automated near-real-time quality control algorithm with improved cloud screening for sun photometer aerosol optical depth (AOD) measurements, *Atmos. Meas. Tech.*, 2019, vol. 12, pp. 169–209.

Hansen, J., Sato, M., Ruedy, R., Lacis, A., and Oinas, V., Global warming in the twenty-first century: An alternative scenario, *Proc. Natl. Acad. Sci. U.S.A.*, 2000, vol. 97, no. 18, pp. 9875–9880.

Holben, B.N., Eck, T.I., Slutsker, I., Tanre, D., Buis, J.P., Setzer, A., Vemote, E., Reagan, J.A., Kaufman, Y.J., Nakajima, T., Lavenu, F., Jankowiak, I., and Smirnov, A., AERONET: A federated instrument network and data archive for aerosol characterization, *Remote Sens. Environ.*, 1998, vol. 66, no. 1, pp. 1–16.

Holben, B.N., Tanré, D., Smirnov, A., Eck, T.F., Slutsker, I., Abuhassan, N., Newcomb, W.W., Schafer, J., Chatenet, B., Lavenue, F., Kaufman, Y.J., Vande Castle, J., Setzer, A., Markham, B., et al., An emerging ground-based aerosol climatology: Aerosol optical depth from AERONET, *J. Geophys. Res.*, 2001, vol. 106, pp. 12067–12097.

Horvath, H., Kasahara, M., Tohno, S., Olmo, F.J., Lyamani, H., Alados-Arboledas, L., Quirantes, A., and Cachorro, V., Relationship between fraction of backscattered light and asymmetry parameter, *J. Aerosol Sci.*, 2016, vol. 91, pp. 43–53.

Imashev, S.A., Methodology for calculating the Ångström parameter and atmospheric turbidity coefficient according to photometric measurement data, *Vestn. Kyrg.-Ross. Slavyanskogo Univ.*, 2012, vol. 12, no. 4, pp. 175–178.

Ionov, D.V. and Poberovskii, A.V., Variability of nitrogen oxides in the atmospheric surface layer near Saint Petersburg, *Russ. Meteorol. Hydrol.*, 2020, vol. 45, no. 10, pp. 720–726.

Jung, C.H., Um, J., Lee, J.Y., et al., Sensitivity analysis of the angstrom exponent for multimodal aerosol size distributions, *Asia-Pac. J. Atmos. Sci.*, 2013, vol. 49, pp. 625–634.

Mikhailov, E.F., Vlasenko, S.S., Podgorny, I.A., Ramanathan, V., and Corrigan, C.E., Optical properties of soot-water drop agglomerates: An experimental study, *J. Geophys. Res.*, 2006, vol. 111.

Rienecker, M.M., Suarez, M.J., Gelaro, R., Todling, R., Bacmeister, J., Liu, E., Bosilovich, M., Schubert, S.D., Takacs, L., Kim, G.-K., Bloom, S., Chen, J., Collins, D., Conaty, A., da Silva, A.M., et al., MERRA: NASA's modern-era retrospective analysis for research applications, *J. Clim.*, 2011, vol. 24, no. 14, pp. 3624–3648.

Schuster, G.L., Dubovik, O., and Holben, B.N., Angstrom exponent and bimodal aerosol size distributions, *J. Geophys. Res.*, 2006, vol. 111, no. D7.

Smith, S.J. and Bond, T.C., Two hundred fifty years of aerosols and climate: the end of the age of aerosols, *Atmos. Chem. Phys.*, 2014, vol. 14, no. 2, pp. 537–549.

Stefan, S., Mihai, L., Nicolae, D., and Boscornea, A., Angstrom turbidity in the lower layers of the troposphere, *Environ. Eng. Manage. J.*, 2011, vol. 10, pp. 133–138.

Sviridenkov, M.A., Verichev, K.S., Vlasenko, S.S., Emilenko, A.S., Mikhailov, E.F., and Nebos'ko, E.Yu., Retrieval of atmospheric aerosol parameters from data of a three-wavelength integrating nephelometer, *Atmos. Oceanic Opt.*, 2014, vol. 27, no. 3, pp. 230–236.

Sviridenkov, M.A., Mikhailov, E.F., and Nebos'ko, E.Yu., Parameterization of asymmetry factor of atmospheric aerosol scattering phase function, *Atmos. Oceanic Opt.*, 2017, vol. 30, no. 5, pp. 435–440.

Timofeyev, Y., Virolainen, Y., Makarova, M., Poberovsky, A., Polyakov, A., Ionov, D., Osipov, S., and Imhasin, H., Ground-based spectroscopic measurements of atmospheric gas composition near Saint Petersburg (Russia), *J. Mol. Spectrosc.*, 2016, vol. 323, pp. 2–14.

Virkkula, A., Backman, J., Aalto, P.P., Hulkkonen, M., Riuttanen, L., and Nieminen, T., dal Maso, M., Sogacheva, L., De Leeuw, J., and Kulmala, M. Seasonal cycle, size dependencies, and source analyses of aerosol optical properties at the SMEAR II measurement station in Hyytiälä, Finland, *Atmos. Chem. Phys.*, 2011, vol. 11, pp. 4445–4468.

Vlasenko, S.S., Volkova, K.A., Ionov, D.V., et al., Variation of carboneceous atmospheric aerosol near St. Petersburg, *Izv., Atmos. Ocean. Phys.*, 2019, vol. 55, no. 6, pp. 619–627.

Vlasenko, S.S., Ivanova, O.A., Ryshkevich, T.I., and Mikhailov, E.F., Estimation of spatial distribution of potential sources of carbonaceous aerosol from local measurements near St. Petersburg, *Izv., Atmos. Ocean. Phys.*, 2023, vol. 59, no. 6, pp. 685–694.

Volkova, K.A., Poberovskii, A.V., Timofeev, Yu.M., et al., Aerosol optical characteristics retrieved from CIMEL Sun photometer measurements (AERONET) near St. Petersburg, *Atmos. Oceanic Opt.*, 2018, vol. 31, no. 6, pp. 635–641.

Volkova, K.A., Anikin, S.S., Mikhailov, E.F., et al., Seasonal and daily variability of aerosol particle concentrations near St. Petersburg, *Atmos. Oceanic Opt.*, 2020, vol. 33, no. 5, pp. 524–530.

Weber, P., Petzold, A., Bischof, O.F., Fischer, B., Berg, M., Freedman, A., Onasch, T.B., and Bundke, U., Relative errors in derived multi-wavelength intensive aerosol optical properties using cavity attenuated phase shift single-scattering albedo monitors, a nephelometer, and tricolour absorption photometer measurements, *Atmos. Meas. Tech.*, 2022, vol. 15, pp. 3279–3296.

Zhao, G., Zhao, C., Kuang, Y., Bian, Y., Tao, J., Shen, C., and Yu, Y., Calculating the aerosol asymmetry factor based on measurements from the humidified nephelometer system, *Atmos. Chem. Phys.*, 2018, vol. 18, pp. 9049–9060.